Packet-based feedback control of electrical drive and its application to trajectory tracking of manipulator

AUTHOR(S):

Mochiyama, Shiu; Hikihara, Takashi

CITATION:

Mochiyama, Shiu ...[et al]. Packet-based feedback control of electrical drive and its application to trajectory tracking of manipulator. International Journal of Circuit Theory and Applications 2019, 47: 612-632

ISSUE DATE:

2019-04

URL:

http://hdl.handle.net/2433/240877

Packet-based feedback control of electrical drive and its application to trajectory tracking of manipulator

Shiu Mochiyama* and Takashi Hikihara

Department of Electrical Engineering, Kyoto University, Kyoto-shi, 615-8510 Japan
*E-mail: s-mochiyama@dove.kuee.kyoto-u.ac.jp

Abstract

In systems disconnected from the external grid, such as mobile robots and vehicles, the effective use of renewables and energy harvesting techniques helps a longer operation with less weight and space for batteries. Power packet dispatching system is a promising measure to manage the complex power flow created by such distributed power sources of various profiles. In the system, power is transferred as a pulse, and information tag is attached to the pulse power in voltage waveforms. The physical integration of power and information realizes a smooth inclusion of sources and loads of different profiles and their decentralized operation. This paper discusses the application of the system to load control. We propose a decentralized packet-based feedback control scheme. The successful operation of the proposed scheme is confirmed by an application to an electrical drive. In addition, the application to trajectory control of 2-degree-of-freedom manipulator reveals the possibility of a peak-power reduction based on a demand response operation of the proposed scheme. The results contribute to a realization of decentralized flow control of power packets based on the convenience of both the sources and the loads.

keywords: power packet, feedback control, electrical drive, manipulator, experiment

1 Introduction

Distributed power sources such as renewables and energy harvesting techniques have been introduced to a wide variety of systems, including robots [1], electric vehicles [2, 3], and aircrafts [4]. Such systems are disconnected from the external grid due to their mobility. Under the limitation of power available, the introduction of renewables and energy harvesting techniques provides many advantages, including a longer operation and a reduction of the weight and volume used for large batteries.

Here, the main challenge toward the introduction of distributed sources is the management of the sources and loads of different and time-varying profiles. A promising measure is their decentralized control with the help of Information and Communication Technologies (ICT) [5–7]. In a system consisting of many elements, a decentralized scheme is more suitable for their control than a centralized one. Due to the limited capacity of computation and communication, a centralized scheme faces a degradation of performance as the number of elements increases.

As a possible realization of decentralized power distribution systems, the power packet dispatching system has been proposed and investigated actively [8–10]. In the system, power and information are transferred in an integrated form called power packet. Figure 1 (a) shows the configuration of a power packet. Power is transferred as a pulse called payload, and an information tag is attached to each payload as a voltage waveform without current. Then the power packets are transferred to their destination loads through a network of power routers, as shown in Fig. 1 (b). On a power line, power packets from different sources are completely distinguished in time-domain, which is called a Time Division Multiplexing (TDM) method. Each power packet can be identified by the attached tag. Because of this physical separation of power transfer, individual pairs of sources and loads do not interact each other. Therefore, the system can attach/detach sources and loads of different profiles smoothly and let them operate flexibly in a decentralized way [11].

Now, in the power packet dispatching system, power is processed as a digital quantity. That is, the power supply is discretized in time and quantity. It is completely different from the conventional systems, where power flow is controlled by a regulation of continuous current flow using power converters. Digital control techniques have been investigated actively and proved to have many advantages over the analog counterpart [12]. In addition, as digital processors have become available at a reasonable price, they are now utilized in distributed and decentralized control systems. However, the existing theories focus on how to generate digital *signal*; there have been few studies on the digitization of the *physical* input itself.

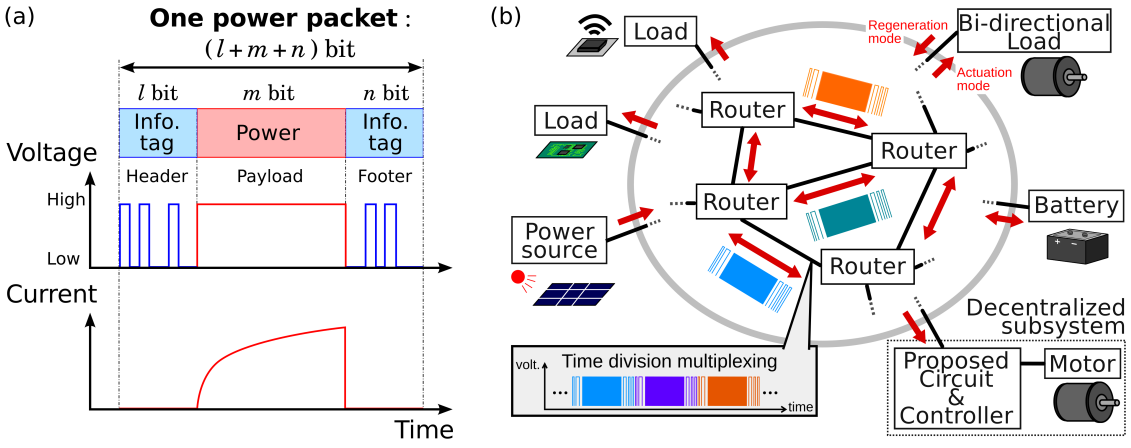

Figure 1: Power packet dispatching system. (a) Configuration of power packet. (b) Dispatching network.

In order to adopt the power packet dispatching system in real-world applications, a novel framework for packet-based control must be established.

In control, feedback information, which is obtained through observations of the environment, is essential for a good performance in a changing surrounding condition. In the case of the power packet dispatching system, the feedback information is utilized in controlling a flow of every power packet. Now note that, as is also mentioned above, our interest is on a decentralized management of the power flow between multiple distributed sources and loads. Therefore, there is no central brain that collects all the feedback information and generates the signal on how to transfer every power packet. Instead, the routers distributed in a dispatching network are required to *think* on its own about how to operate based on feedback information available locally. This perspective has scarcely been investigated in the power packet dispatching system so far (see Section 1.1). Most previous studies were based on passive operation of routers; the routers distribute power packets according only to the tag information, which is determined and attached at the source side.

With these motivations, we develop a packet-based control scheme using feedback information that is implemented into the routers and operates in a decentralized manner. The contribution of this paper is listed as follows.

- A packet-based feedback control scheme is developed (Section 2). As shown at right bottom in Fig. 1 (b), the scheme is implemented as a dispatching circuit and its controller. They are regarded as an end-node subsystem in a general power packet dispatching system. They regulate the supply of power packets by a density modulation using the state feedback from its load. In addition, the regulation is performed in a decentralized way; that is, the processing of power and information is conducted partially at the receivers, not only at the senders.

- Performance analysis of the proposed feedback scheme is presented (Section 2). The performance is evaluated in comparison with a conventional feedback control system with continuous power supply. It is shown that the performance degradation due to the introduction of the power packetization can be estimated quantitatively in advance. Then, we conduct numerical simulations and experiments of an electric drive with the proposed subsystem (Section 3). It is confirmed that the performance degradation is sufficiently small and does not prevent the achievement of angle control.

- The proposed scheme is applied to trajectory control of manipulator (Section 4). Each joint motor of the manipulator is controlled by a dedicated decentralized subsystem. The successful trajectory control is confirmed through experiments. In addition, a demand response operation of the subsystems is presented. Under the limitation of instantaneous power available, the joint motors are controlled by their own subsystems to share the power. This setting is for demonstrating that the proposed system can create the flow of power packets based on the constraints of the sources, as well as of the loads. This operation is realized as a communication between neighbor subsystems.

1.1 Related works

In this subsection, we present some related works regarding the application of the power packet dispatching to load control.

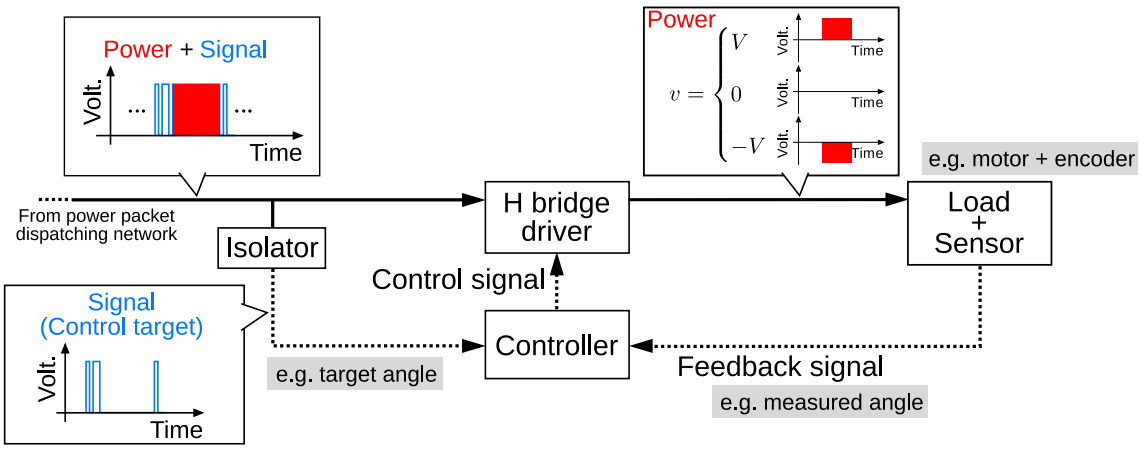

Figure 2: Configuration for packet-based feedback control.

So far, there have been some studies on the load control in *open-loop* supply of packetized power. For example, an open-loop power regulation by power packet density modulation has been proposed in [13]. The fundamental idea of this paper is inspired by the study, regarding the use of dynamic quantization (Section 2). Besides that, in our previous paper [14], packet-based control is applied to trajectory control of a manipulator. However, there have been only limited results on a feedback control of power packet supply, in spite of the importance of feedback control in engineering applications. In addition, the feedback scheme developed in this paper is not just a feedback version of the open-loop regulation [13] with a trivial modification of software. In the previous proposal, the destination of power is determined at the generation of power packets. On the contrary, we propose the decentralized way. This decentralization is more suitable for our target systems that consist of multiple sources and loads.

The close-loop control of power packet supply is partially discussed in [15]. In fact, the concept of the decentralized implementation of subsystems for load control is first proposed there. However, the control scheme in [15] is dedicated to angle control of a stepper motor. Taking advantages of a particular structure of stepper motors, the scheme achieved the angle control only by the close-loop selection of a supply phase. On the contrary, in this paper, the power packet density modulation realizes the regulation of instantaneous power. This method is applicable not only to motors but also to general systems that can be identified as a state-space model.

A part of the experimental results in Section 4 is reported in [16]. It is extended in this paper by presenting additional results and discussion on the achievement of angle control and the demand response operation by packet-based feedback control. In addition, the detailed analysis of the control scheme itself is provided for the first time in this paper.

2 Packet-based feedback control scheme

Figure 2 shows the configuration for the proposed packet-based feedback control. This configuration corresponds to an endpoint node in a whole dispatching system, and we call it simply as a subsystem throughout this paper. The input power packets can come from any power sources in the network through multiply connected routers. A power packet transfers both power and signal. The power is transferred as a sequence of pulses called payloads. The polarity of the input is controlled by an H bridge module [1]. The signal is transferred by a header of a power packet, i.e. an information tag just before a payload (see Fig. 1 (a)). The signal includes a control target of the destination load. Note that the isolator module works as an interface between the power line and the signal line. It blocks the current and pass only the voltage waveforms of the tag to the controller board.

Now we assume that the power packets are produced by a constant voltage source. Then we define the input of the controlled plant P is input voltage v. In many existing systems, the input is regulated by circuit switching using Pulse Width Modulation (PWM). On the contrary, in this paper, we adopt a Pulse Density Modulation (PDM) [17, 18]. That is, the input is regulated based on the number of pulses in a unit time duration. Here, regarding the configuration of a power packet, we assume the followings:

- A payload is a minimum unit of power supply, and the polarity of the motor input does not change during a payload.

[1] Of course, when the load does not require the change of the polarity, the H bridge can be replaced by a single switch.

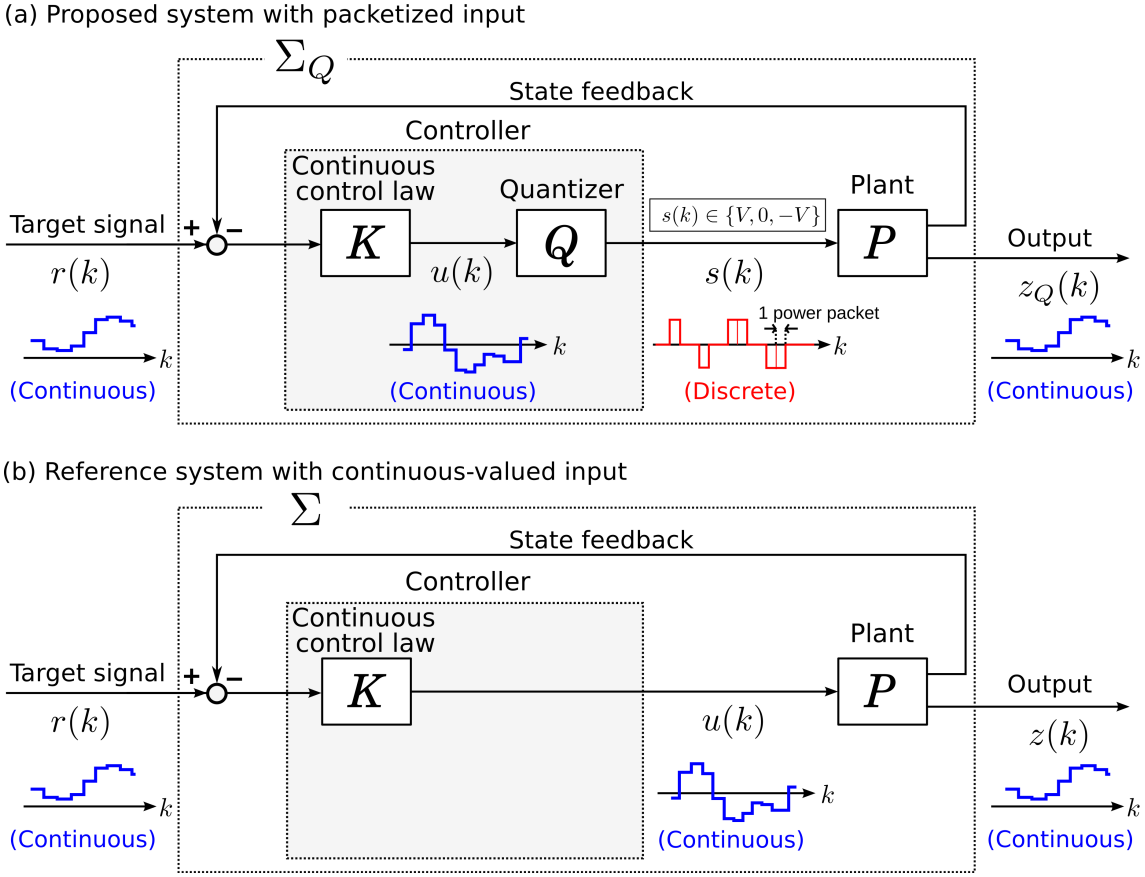

Figure 3: Packet-based feedback control system, Σ_Q, and its reference system with continuous input, Σ.

- The length and the voltage of power packets are fixed at T and V, respectively.
- For discrete time $k = 1, 2, \cdots$, the time slot for the k-th power packet is expressed by $t = [(k-1)T, kT)$ in continuous time.

In addition, in the controller design of this section, we assume that the length of information tags is sufficiently small to ignore. This assumption is based on the recent development of wide band-gap devices and their driving techniques, which realize a fast switching without remarkable loss [19, 20]. With the definitions and assumptions above, we denote the input voltage of k-th time slot by $s(k) \in \{+V, 0, -V\}$. Note that $s(k)$ $(k = 1, 2, \cdots)$ is actually a signal generated by the controller. The voltage input $v = s(k)$ is realized by an H bridge driver, which alters the polarity of the payload supply according to a control signal $s(k)$ given by the controller.

The signal $s(k)$ is generated at every power packet input $t = kT$, based on a target signal extracted from an information tag and a feedback signal from the load. In this paper, we consider the control system consisting of a conventional continuous-valued control scheme K and a signal quantizer Q. Figure 3 shows the configuration of the control scheme to generate $s(k)$. The control scheme determines the supply of k-th power packet, $s(k)$, at the arrival of the power packet. K generates a continuous-valued sequence $u(k)$ based on a state feedback and a target. Then, Q converts $u(k)$ into discrete-valued signal $s(k) \in \{+V, 0, -V\}$.

In this paper, we adopt an Optimal Dynamic Quantizer (ODQ) for Q [21, 22]. The quantizer is designed to be optimal in the sense that it minimizes the effect of the quantization error on the output of the controlled plant. The design of an optimal Q requires the state space model of the controlled plant P and the continuous-valued control scheme K. We consider a linear, time-invariant, and single-input-single-output (SISO) [2] plant P expressed by a discrete-time state space representation

$$P : \begin{cases} x_{\mathrm{p}}(k+1) = A_{\mathrm{p}}\, x_{\mathrm{p}}(k) + B_{\mathrm{p}} s(k) \\ y(k) = C_{1\mathrm{p}}\, x_{\mathrm{p}}(k) \\ z(k) = C_{2\mathrm{p}}\, x_{\mathrm{p}}(k) \end{cases}, \tag{1}$$

where $x_{\mathrm{p}} \in \mathbf{R}^n$, $y \in \mathbf{R}^m$ and $z \in \mathbf{R}$ represent the state, the feedback signal, and the output for evaluation, and $A_{\mathrm{p}} \in \mathbf{R}^{n \times n}$, $B_{\mathrm{p}} \in \mathbf{R}^n$, $C_{1\mathrm{p}} \in \mathbf{R}^{m \times n}$, and $C_{2\mathrm{p}} \in \mathbf{R}^n$ are constant coefficient matrices. The state space model of

[2] The assumption of linearity and SISO is just for the simplicity of the expression. Q can be obtained for nonlinear systems of multiple input/output [21, 23].

K is expressed by

$$K : \begin{cases} x_{\mathrm{k}}(k+1) = A_{\mathrm{k}}\, x_{\mathrm{k}}(k) + B_{1\mathrm{k}} r(k) + B_{2\mathrm{k}} y(k) \\ u(k) = C_{\mathrm{k}}\, x_{\mathrm{k}}(k) + D_{1\mathrm{k}} r(k) + D_{2\mathrm{k}} y(k) \end{cases}, \tag{2}$$

where $x_{\mathrm{k}} \in \mathbf{R}^l$ and $r \in \mathbf{R}$ represent the state and the target signal, and $A_{\mathrm{k}} \in \mathbf{R}^{l\times l}$, $B_{1\mathrm{k}} \in \mathbf{R}^l$, $B_{2\mathrm{k}} \in \mathbf{R}^{l\times m}$, $C_{\mathrm{k}} \in \mathbf{R}^l$, $D_{1\mathrm{k}} \in \mathbf{R}$, and $D_{2\mathrm{k}} \in \mathbf{R}^m$ are constant coefficient matrices.

Now let us consider a dynamic quantizer Q of a dimension d in the following form:

$$Q : \begin{cases} \xi(k+1) = A_{\mathrm{q}}\, \xi(k) + B_{1\mathrm{q}} u(k) + B_{2\mathrm{q}} s(k) \\ s(k) = q(C_{\mathrm{q}}\, \xi(k) + u(k)) \end{cases}, \tag{3}$$

where $\xi \in \mathbf{R}^d$ represents the state of the quantizer and the function $q(\cdot)$ is a static quantizer of quantization interval V. The matrices $A_{\mathrm{q}} \in \mathbf{R}^{d\times d}$, $B_{1\mathrm{q}} \in \mathbf{R}^d$, $B_{2\mathrm{q}} \in \mathbf{R}^d$ and $C_{\mathrm{q}} \in \mathbf{R}^d$ are the design parameters of Q.

In [24, 25], a numerical method is proposed to find the design parameters of Q which minimizes the difference of the input/output relationship between the system with quantizer Σ_Q and the system without quantizer Σ. A brief review of the optimization procedure is presented below. Let $\tau \in \mathbf{N}_+ \cup \{\infty\}$ be a (discrete) time interval over which the performance of Q is evaluated. A sequence of the target over τ is defined as $R := \{r(0), r(1), \cdots, r(\tau)\}$. Then the output sequence of the quantized system Σ_Q for a set of an initial state and a input sequence $(x(0), R) \in \mathbf{R}^n \times \mathbf{R}^{\tau+1}$ is defined as

$$Z_Q(x(0), R) := \{z_Q(k, x(0), R) \,|\, k \in \{0, 1, \cdots, \tau\}\}, \tag{4}$$

where z_Q is the k-th output. In the same way, the k-th output of the ideal system Σ and its sequence over τ are defined as $z(k, x(0), R)$, $Z(x(0), R)$, respectively. The parameters of Q is determined so that the maximum output error

$$E(Q) := \sup_{(x(0),R)\in\mathbf{R}^n\times\mathbf{R}^\tau} \|Z_Q(x(0), R) - Z(x(0), R)\| \tag{5}$$

$$= \sup_{(x(0),R)\in\mathbf{R}^n\times\mathbf{R}^\tau} \left\{ \sup_{k\in\{0,1,\cdots,\tau\}} \|z_Q(k, x(0), R) - z(k, x(0), R)\| \right\} \tag{6}$$

is minimized, where $\|\cdot\|$ represents ∞-norm.

Once parameters of Q are determined, $E(Q)$ indicates the upper bound of the output error. In the numerical analysis in Section 3, the control performance is evaluated based on the value of $E(Q)$.

Now note that in the power packet dispatching system, the input of P is limited to three levels $\{V, 0, -V\}$, while the output of the static quantizer q in Eq. (3) can take any integer multiple of V, i.e. $aV (a \in \mathbf{Z})$. The gap is filled by a numerical optimization under an additional constraint on the upper bounds of the input-output gain $\gamma_1 (\geq 1)$ and the error-output gain $\gamma_2 (\geq 1)$ [24]. The output of Q satisfies the condition

$$|s(k)| \leq \gamma_1 U_{\max} + \gamma_2 \frac{V}{2}, \tag{7}$$

where $U_{\max}$ represents the maximum absolute value of the input sequence of Q:

$$U_{\max} := \max_{k\in\{0,1,\cdots\tau\}} \|u(k)\|. \tag{8}$$

For example, if we know that $U_{\max} < V$ holds, then $\gamma_1 = 1$ and $\gamma_2 = 2$ give $|s(k)| < 2V$ $(k = 0, 1, \cdots \tau)$. That is, the quantized output takes a value only from $\{V, 0, -V\}$. For the design of Q in Section 3, we confirm that the output of the continuous-valued controller, $u(k)$, does not exceed V by preliminary numerical simulations.

Here a comment is given regarding the input/output stability of the whole system Σ_Q. Suppose that the ideal reference system Σ is bounded-input bounded-output (BIBO) stable. That is, if there exists $\mu \in \mathbf{R}_{\geq 0}$ that satisfies $|r(k)| < \mu$ for any sequence $\{r(k)\}$ and for all time $k = 0, 1, 2, \cdots$, then there exists $M = M(\mu) \in \mathbf{R}_{\geq 0}$ that satisfies $|z(k)| < M(\mu)$ for all time $k = 0, 1, 2, \cdots$. Under this condition, it is obvious from Eq. (6) that if $\{r(k)\}$ is bounded by μ, the output of Σ_Q is also bounded by $M_Q := M(\mu) + E(Q)$. That is, the packetization of the supply does not violate the BIBO stability of P and K.

3 Angle control of single motor

In this section, we discuss angle control of a motor with the proposed subsystem. A numerical performance analysis and its experimental verification are given. To build the numerical models for the performance analysis, we first present the experimental setup of P and K, determine the parameters of their models, and design the quantizer Q based on the numerical models. Then, we numerically confirm the performance of the proposed control scheme with the models and the designed quantizer. Lastly, we confirm the achievement of a successful angle control with the experimental setup.

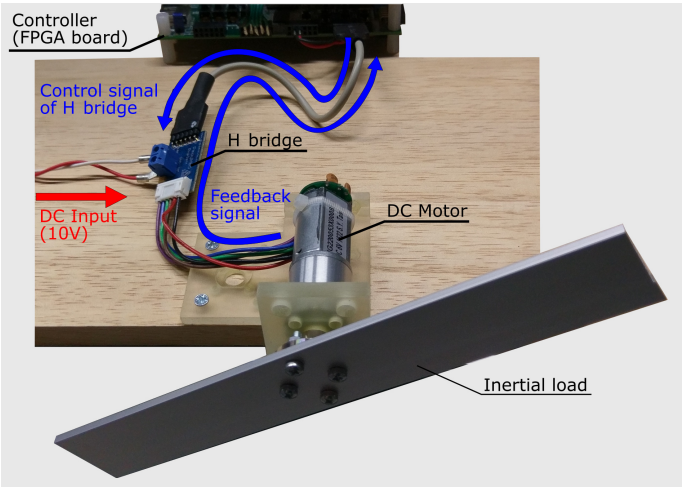

Figure 4: Experimental setup for angle control of single dc motor by proposed packet-based feedback scheme.

Table 1: Specifications of DC brushed motor used in experiment (picked up from official data sheet [26]).

Item	Value
Rated voltage	6 V dc
Coil resistance	3.33 Ω
Torque constant	0.22 N m A^{-1}
Gear ratio	52.734
Backlash	Max. 3°

3.1 Experimental Setup and Design of Quantizer

We consider close-loop angle control of a dc brushed motor by power packets. This kind of motor is supplied by dc power through its two-port terminal. The direction of the rotation is controlled by changing the polarity of the supply. An H bridge driver is often used to alter the polarity.

Now, let v, i, θ, and ω be the input voltage across the dc input port, the current flowing through the motor windings, the rotation angle, and the rotation velocity, respectively. The circuit equation of a dc brushed motor is expressed by

$$L\frac{\mathrm{d}i}{\mathrm{d}t} + Ri + K_{\mathrm{e}}\omega = v, \tag{9}$$

where K_{e}, L, and R denote a back electromotive force constant, inductance of the winding, and resistance of the winding, respectively. The equation of motion of the motor is then expressed by

$$J\dot{\omega} + b\omega = K_{\mathrm{t}}i, \tag{10}$$

where K_{t}, J, and b denote a torque constant of the motor, a moment of inertia around the motor shaft, and friction constant of the motor, respectively. From the Eqs. (9) and (10), the input and output of P are defined as the input voltage v and the angle θ.

Figure 4 shows the experimental setup. The setup consists of a geared dc motor equipped with a magnetic encoder [26], its dedicated H bridge driver [27], and a FPGA board as the controller. Table 1 shows the specification of the motor. The encoder can identify the rotor position in 12 levels; therefore, taking the gear ratio into consideration, the resolution is approximately $0.57°(\simeq 360°/(12 \times 53))$. An inertial load of cuboid shaped aluminum is attached to the shaft of the motor. The moment of inertia of the load is 2.5×10^{-4} kg m^2. With these values and Eqs. (9) and (10), the parameters of the numerical model for P are determined as shown in Appendix A.

The voltage of the power source V is set at 10 V. The length of a power packet T is set at 800 μs. The target angle of the motor is set as a step-like signal

$$r(k) = \begin{cases} 54° & (k \geq 0) \\ 0° & (k < 0) \end{cases}. \tag{11}$$

Now note that we transfer power and target angle signals separately in the experiments of this section. The target angle trajectory is stored in a memory and transferred to the control scheme at every time instant

Table 2: Designed parameters of Q obtained by optimization.

Parameter	Value
A_q	0.9969
B_{1q}	−0.9985
B_{2q}	0.9985
C_q	−0.9985

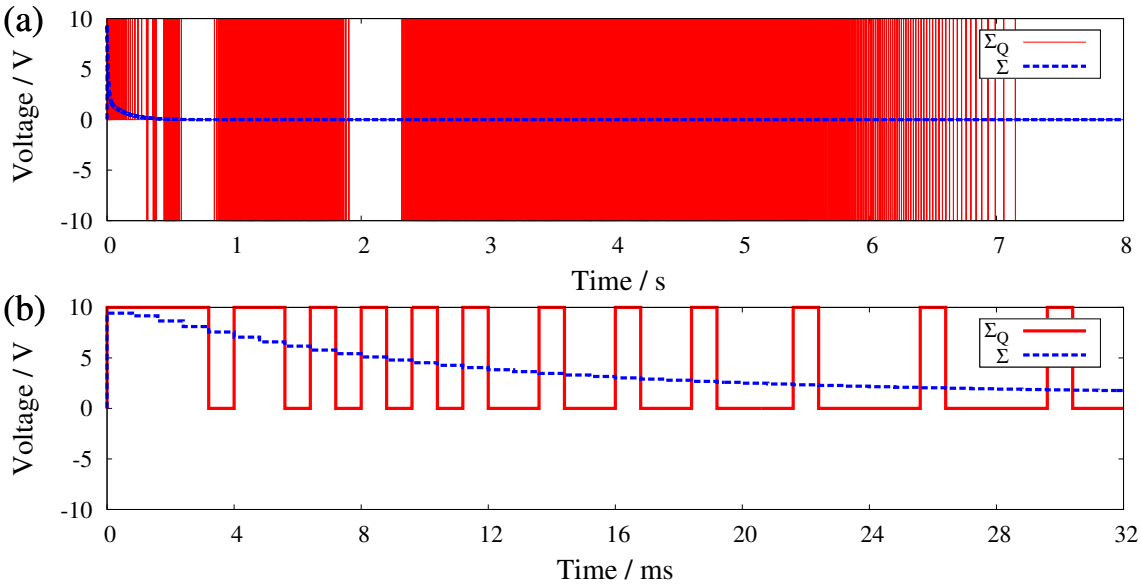

Figure 5: Input voltage of motor obtained through numerical simulations. (a) Packet sequence $s(k)$ (red line) and the continuous input voltage (blue line). (b) Enlarged view of (a) in the time interval of 0–32 ms.

$t = kT$ $(k = 1, 2, \cdots)$. This simplification of the setup is for focusing on the performance analysis of the motor control by digitized power. The transfer of both power and information is confirmed in the experiments of manipulator control in Section 4.

For K, we adopt a Proportional-Integral-Differential (PID) controller. The PID gains are determined so that the motor reaches the target angle within a second and an overshoot is as small as possible. The gain parameters of proportional, integral and derivative terms are determined as $K_p = 10$, $K_i = 5$, and $K_d = 1$, respectively. Their state-space model is presented in Appendix A.

Now let us design an optimal quantizer Q based on the models of P and K. Throughout this paper, we use a MATLAB software for designing the parameters by numerical optimization [22] with SeDuMi, a solver package for MATLAB [28]. We conducted the optimization under the condition of the gains $\gamma_1 = 1$ and $\gamma_2 = 2$, the time interval $\tau = 200$, and the dimension $d = 1$. Table 2 shows the parameters obtained by the optimization. With the parameters, the maximum output error for $t \to \infty$ is computed as $E = 0.3266°$. That is, the difference between the ideal system and the quantized system is expected to be always less than or equal to E.

3.2 Results of numerical simulation

In this subsection, the results of numerical simulations are presented. We conduct simulations both with the quantized system Σ_Q and the unquantized system Σ to give an evaluation based on their comparison.

First, let us confirm the packetized input. Figure 5 shows the results of the simulation regarding the input voltage. In Fig. 5 (a), the voltage in the ideal case (blue line) drew a decaying curve, while the power packet input (red line) represented them by three levels. This is shown in detail in Fig. 5 (b), where the density of "plus" input varied according to the continuous voltage.

Now we check the achievement of the angle control. Figure 6 shows the results of the simulation regarding the angle trajectories. Figure 6 (a) indicates that the angle in quantized system Σ_Q approaches the target asymptotically. In addition, the angle trajectory is almost same with that of continuous input case shown in Fig. 6 (b). In fact, Fig. 6 (c) shows that their difference is below the theoretical bound 0.3266° [3].

From these results, we can confirm that the designed quantizer Q successfully generated a sequence of power packets $s(k)$ that approximated the continuous signal $u(k)$. The digitization of the power supply did

[3] Note that Fig. 6 (c) does not show the difference from the target angle.

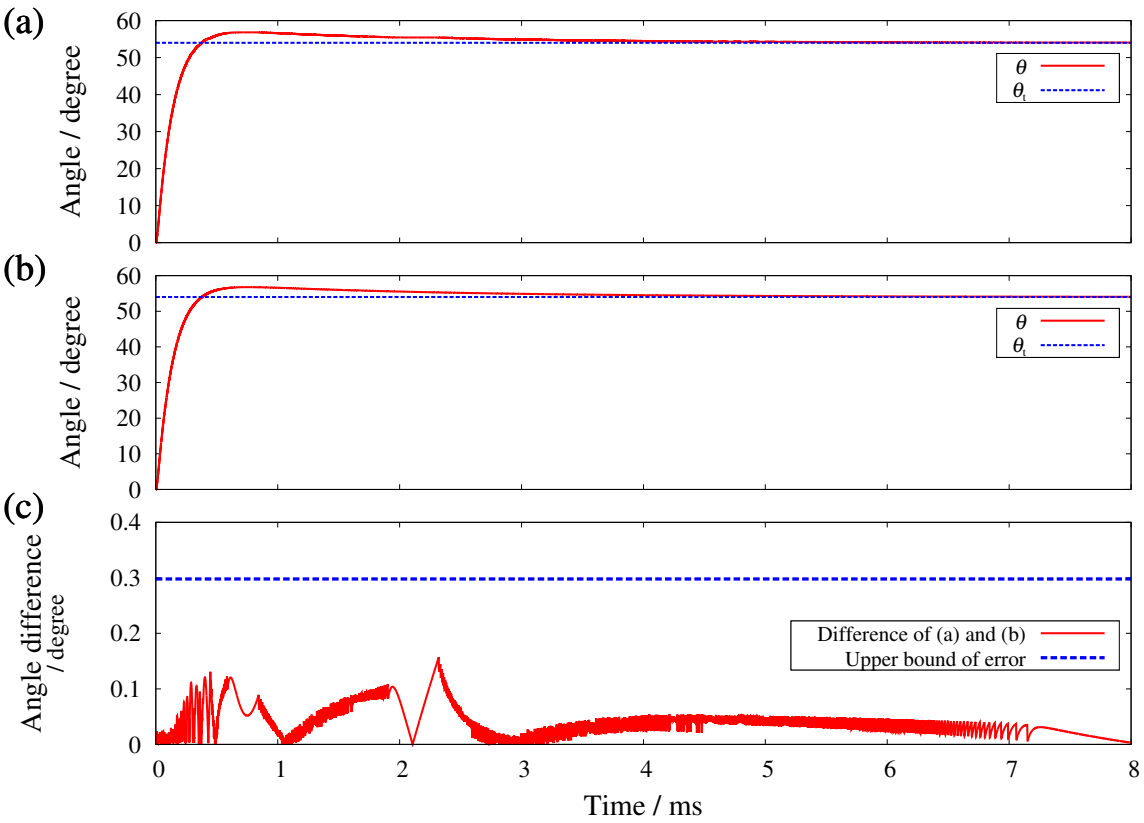

Figure 6: Angle trajectory obtained through numerical simulations. (a) Angle trajectory with power packet input. (b) Angle trajectory with continuous (ideal) input. (c) Difference between (a) and (b).

not have much effect on the control performance. Moreover, the amount of the effect was below the upper bound estimated in advance.

The performance of the packet-based system is in fact comparable to that of conventional systems. It is confirmed by a comparison with a system based on pulse width modulation (PWM), which is often used in applications such as a robot manipulator. We conduct a numerical simulation with the same setup except for the replacement of the ODQ with a PWM. We adopt a three-level PWM with the carrier frequency 0.5 kHz and the voltage 10 V. The frequency is selected so that the pulse width at around half duty become consistent with that of the previous simulation. Figure 7 shows the angle trajectory obtained through the numerical simulation. Figure 7 (a) indicates that the angle trajectory is controlled to the target in the similar way with the case with the power packet input. Then the amount of the angle difference from the ideal case is shown in Fig. 7 (b) for both the cases with the PWM and the packet-based scheme. In the comparison between them, the maximum amplitude of the difference and the remaining error after approaching the target angle are both on the same level. These results are satisfactory from our standpoint because they show that the proposed scheme realizes our target without significant loss of performance. Note that our main target is not to improve the precision of the control, but to introduce the advantages that are brought by constituting a dispatching network capable of handling a variety of sources and loads.

3.3 Results of experiment

Next, let us move on to the results of experiments. Figure 8 shows the voltage and current waveforms measured at the input of the motor. The input sequence $s(k)$ in Fig. 8 (a) represents the continuous input of the reference system by a density modulation of three levels. Then, we focus on the enlarged time interval from 0 ms to 32 ms in Figs. 8 (b) and (c). The current pulses appear in the same direction with the sign of $s(k)$. That is, the H bridge module is successfully controlled by the controller. Note that the discontinuous current change at 8 ms in Fig. 8 (c) is not caused by the change of $s(k)$; it is due to the commutation by the brush.

Figure 9 shows the angle trajectory measured in the experiment. Figure 9 (a) indicates that the motor angle reaches the target, drawing the similar curve with the result of the numerical simulation. However, there appears larger angle error compared with the results of numerical simulation. Figure 9 (b) shows

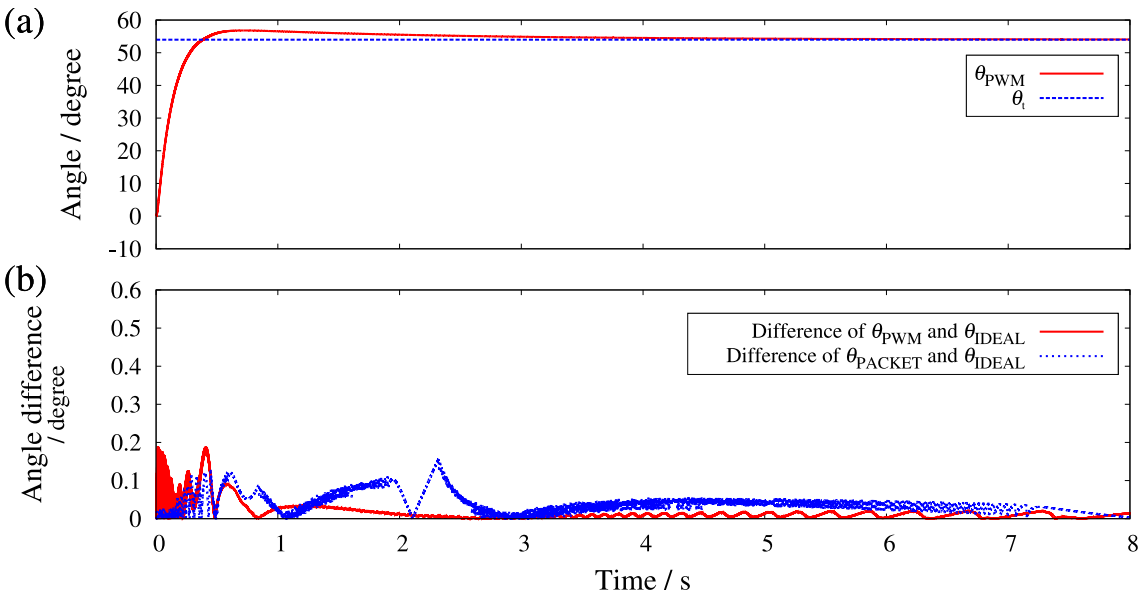

Figure 7: Angle trajectory obtained through numerical simulations with PWM input. (a) Angle trajectory with PWM input. (b) Difference between trajectories with PWM input and with continuous (ideal) input. The blue line in (b) is reproduced from Fig. 6 (b) for reference purpose.

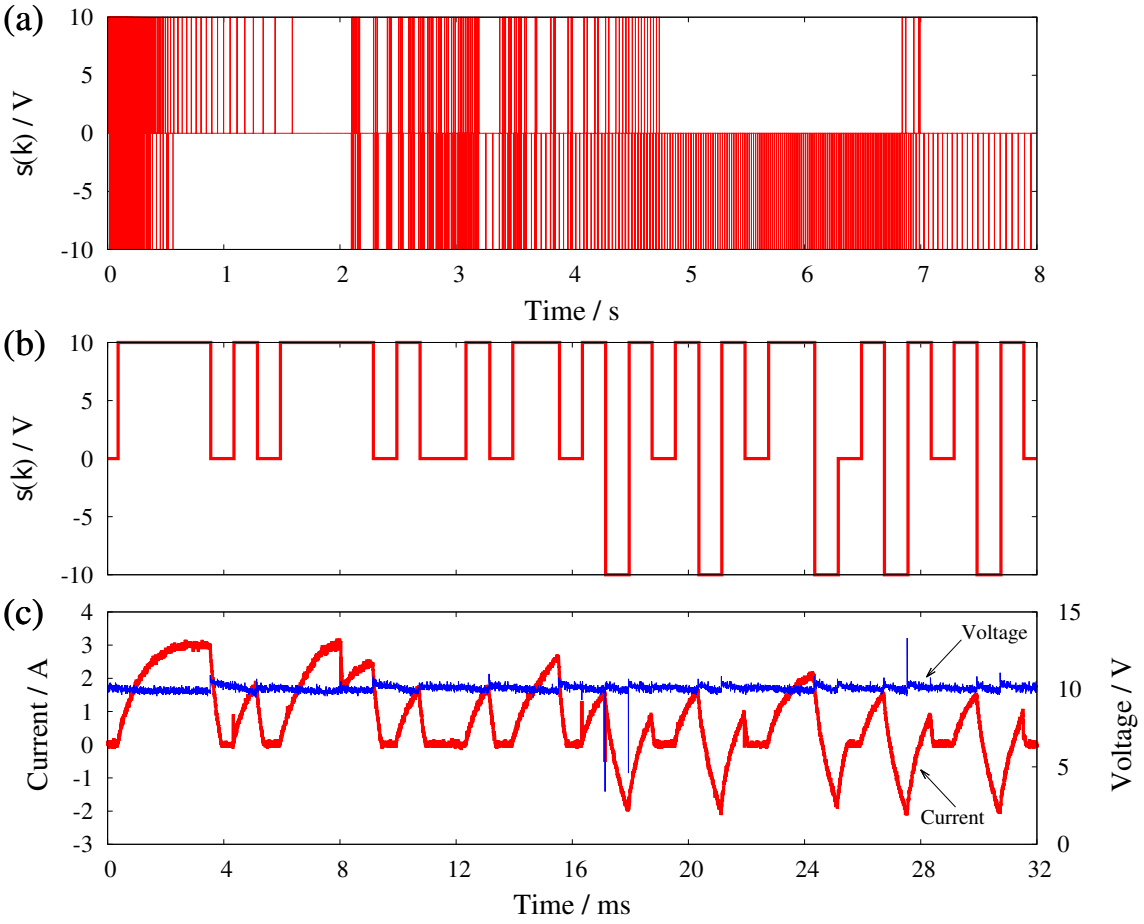

Figure 8: Voltage input sequences and current waveforms measured in experiment. (a) Sequence $s(k)$ of whole experiment. (b) Enlarged view of (a). (c) Voltage and current measured at the input of the motor.

the angle error from the target [4]. Here note that, although we designed the numerical model based on the experimental setup, they have some differences. Due to the linearization in the modeling, the numerical model does not include the following characteristics of the experimental setup:

[4]Note that Fig. 9 (b) does not show the difference from the simulation results.

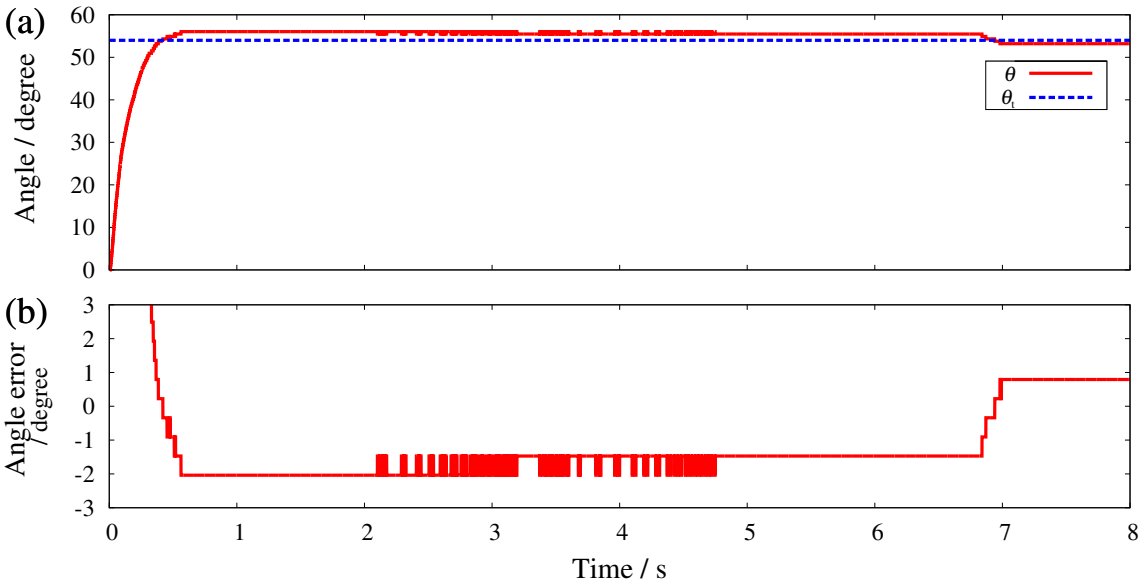

Figure 9: Angle trajectory measured in experiment. (a) Measured trajectory and its target. (b) Difference between the measured trajectory and the target.

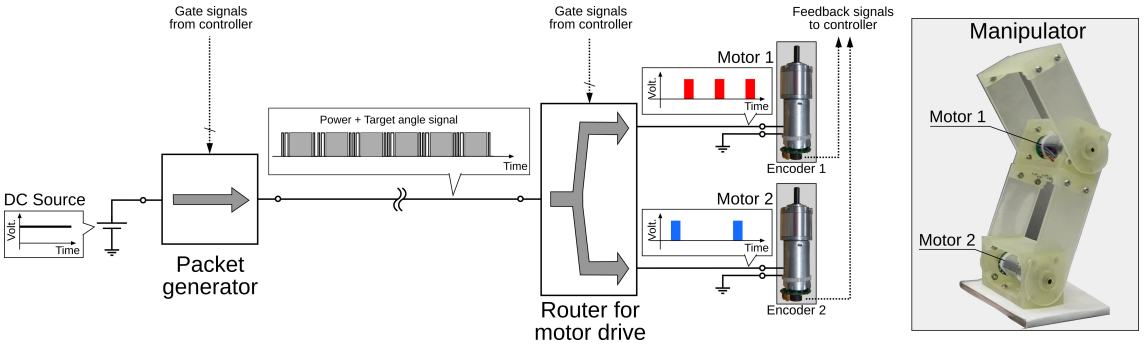

Figure 10: Configuration for trajectory control of manipulator with proposed subsystems.

- The resolution of the encoder is limited by 0.57°.
- The gearbox has a backlash up to 3°.
- The detent torque traps the motor angle at certain positions especially in slow rotation.

In fact, the error in the experimental results can be explained by these modeling difference. In Fig. 9 (a), there remains a constant error in 1–7 s, and then occurs a sudden jump at 7 s. This is caused mainly by the detent torque, which is not included in the numerical model. There also appears a small oscillation in 2–5 s, which is due to the limited resolution of the encoder. Taking them into consideration, we conclude that the angle control was successfully achieved with a packetized power supply. Although we put a priority on the simplicity of the models and accepted these differences, they will be reduced by introducing a more realistic model for P by utilizing a quantizer design method that accepts a nonlinear plant model [23].

4 Trajectory control of manipulator

In this section, we discuss trajectory control of 2-degree-of-freedom manipulator by power packets based on the proposed subsystems for motor control. Decentralized subsystem with a dc brushed motor is implemented into each joint of the manipulator. Power and control signals are transferred in a packetized form, and they are processed by the individual subsystems.

4.1 Experimental setup

Figure 10 shows the configuration for feedback control of manipulator by power packets. It consists of one power source, two joint motors, and a dispatching system between them. The joint motors are the same ones as used in Section 3.

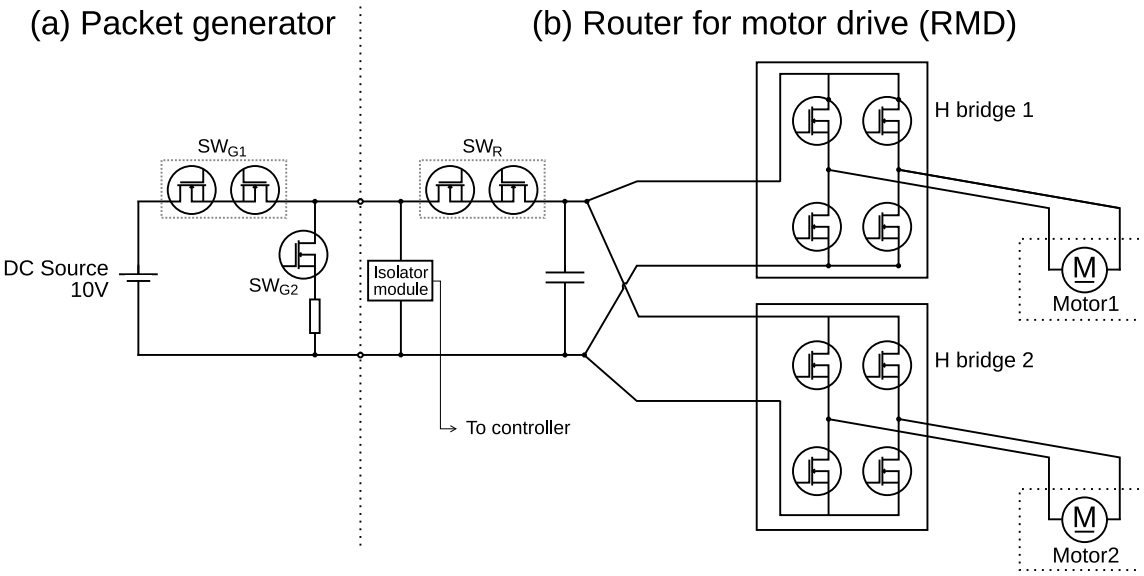

Figure 11: Circuit configuration for manipulator control.

Table 3: Switching table for packet generator.

SW_{G1}	SW_{G2}	Operation
ON	OFF	Output "HIGH"
OFF	ON	Output "LOW"
OFF	OFF	Idling
ON	ON	(Prohibited)

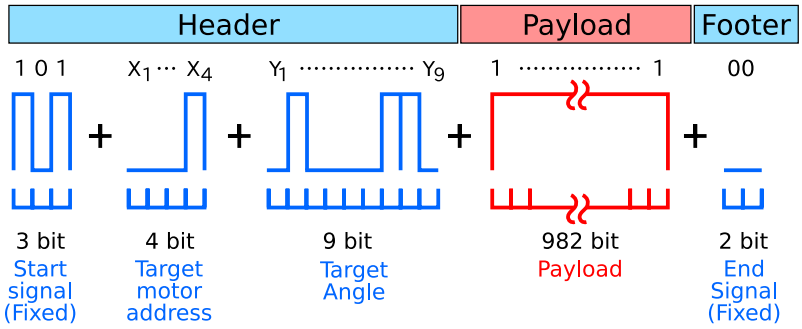

Figure 12: Tag assignment rule for manipulator control.

Figure 11 shows the circuit configuration of the dispatching system. The circuit consists of a packet generator [5] and a Router for Motor Drive (RMD). The packet generator and the RMD have its own controller to turn on/off the switches. The circuits adopt bi-directional switches for future expansion, while we here consider the transfer only on the direction from left to right in the figure. A group of two back-to-back switches is called just a switch throughout this paper.

The packet generator produces a sequence of power packets by circuit switching. Figure 11 (a) shows the circuit configuration of the packet generator. The two switches SW_{G1} and SW_{G2} are controlled in a complementary manner to generate the logic "HIGH" and "LOW" and the payload. Table 3 shows the switching rule of the switches. For logic output in information tags, SW_{G1} is turned on to output "HIGH" and SW_{G2} to output "LOW". For power output during payload, SW_{G1} is kept on and SW_{G2} is kept off.

The voltage of the power source is set at 10 V. The length of a power packet is set at 800 μs. In the experiments, the target angles of the motors are transferred by information tags. Each power packet transfers a target angle of one motor. For $j = 1, 2, \cdots$, the $(2j-1)$-th power packet transfers a target angle of the motor 1, and $(2j)$-th transfers that of the motor 2. Figure 12 shows the signal assignment rule for information tags. The start and end signals of a power packet are represented by fixed sequences. The target motor is indicated by 4 bit: "0000" for the motor 1 and "0001" for the motor 2 [6], where 1 and 0 represent

[5] The packet generator has a similar configuration with what we call a mixer [8]. We call it packet generator in this paper because it has only one source and does not handle power packets from different sources.

[6] The unused 3 bit can be used for a future expansion and/or for another coding technique with more noise immunity, for example.

Table 4: Operation mode of RMD and corresponding switching states. Switching states are represented by a combination of the three states: (SW_R,H bridge 1, H bridge 2). The items with an underscore are prohibited in the setting of case II.

	$s_2(k) = V$	$s_2(k) = -V$	$s_2(k) = 0$
$s_1(k) = V$	(ON,CW,CW)	(ON,CW,CCW)	(ON,CW,0)
$s_1(k) = -V$	(ON,CCW,CW)	(ON,CCW,CCW)	(ON,CCW,0)
$s_1(k) = 0$	(ON,0,CW)	(ON,0,CCW)	(OFF,0,0)

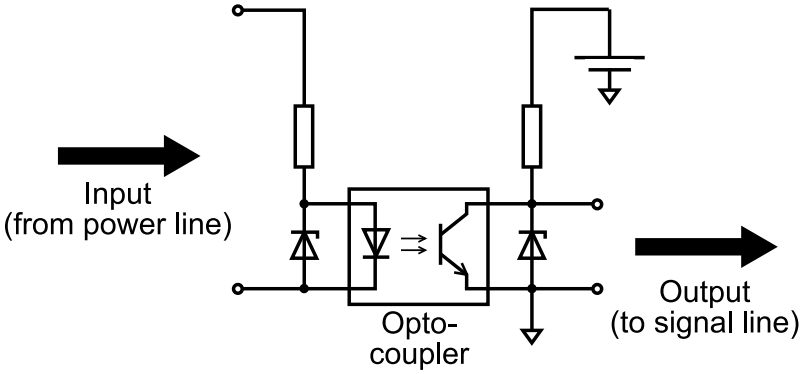

Figure 13: Circuit configuration of isolator module.

Table 5: Gain parameters for PID controllers K_1 and K_2.

Item	Motor 1	Motor 2
K_p	90	30
K_i	30	10
K_d	0	0

Table 6: Designed parameters of the quantizers Q_1 and Q_2.

Item	Motor 1	Motor 2
A_q	0.9972	0.9972
B_{1q}	-0.9986	-0.9986
B_{2q}	0.9986	0.9986
C_q	-0.9986	-0.9986

HIGH and LOW, respectively. Then the following 9 bit expresses the target angle as a binary number: e.g. "000101010" equals to 42°.

The target trajectory of the manipulator is set as sinusoidal waveforms of different amplitude and frequency for the individual joints. The trajectories for discrete time k are defined as

$$\theta_{t,1}(k) = \mathrm{round}(45\sin(2\pi f_1 k)), \quad \theta_{t,2}(k) = \mathrm{round}(-60\sin(2\pi f_2 k)), \tag{12}$$

where the function round$(\cdot)$ maps its argument to the nearest integer. The frequency coefficients are set as $f_1 = 3\times10^{-4}$ and $f_2 = 4\times10^{-4}$. The target angles are stored in the controller of the packet generator as the formulas (12). At every power packet generation, the controller computes a value of that time instant and converts it to a binary to use for a header signal.

The produced power packets are forwarded to the RMD and then distributed to the motors. Figure 11 (b) shows the circuit configuration of the RMD. The RMD is composed of an isolator module to read the information tag and a routing circuit to dispatch power packet to motors. Figure 13 shows the configuration of the isolator module. The isolator module converts a voltage waveform of a tag to a logic input of the controller. The routing circuit consists of a switch and two subsystems for close-loop motor control defined in Section 2 [7]. When a power packet is transferred to the RMD, it first reads the header tag. Until it reads the end of the header, the switch SW_R is kept off to block current. Then, the controllers of the individual subsystems determine the supply of the following payload $s(k)$ based on a PID law and quantizer algorithms. During the payload, SW_R and H bridges are controlled so that the power is supplied

[7] Compared with the previously proposed router [9], the switches to dispatch the input payload to the motors are replaced by subsystems.

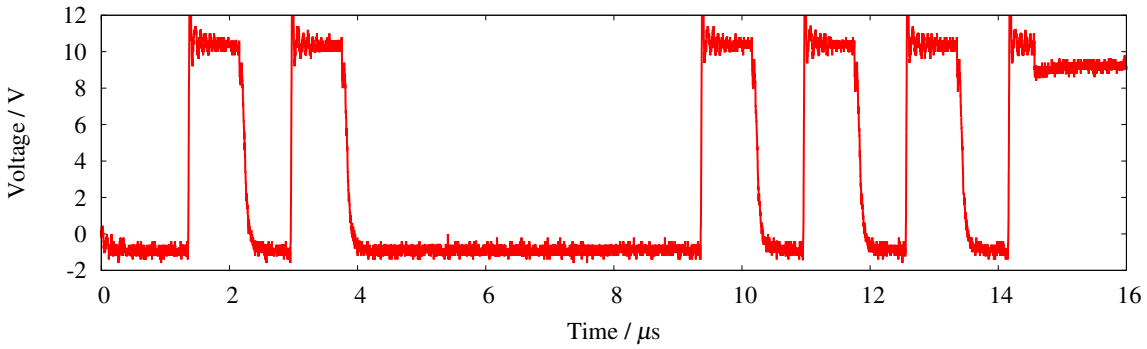

Figure 14: Enlarged view of voltage waveform of information tag.

to the requested motor(s) in the requested polarity. Table 4 shows the operation mode and corresponding switching states. The switching state is kept until the end of the payload. Lastly, when the controller detects the footer signal, all the switches are turned off. This procedure is repeated at every power packet input.

In the tag reading of the RMD, it is important to synchronize the clock of the packet generator and the RMD. In this paper, we adopt an additional wire for this purpose. However, the wire can be removed by introducing an algorithm for autonomous clock synchronization reported in [29].

Now, let us move on to the design of the continuous-valued controller and the quantizer. In the manipulator control, each motor is controlled locally for simplicity of the controller design. The PID scheme and the quantizer for the motor i ($i = 1, 2$) are called K_i and Q_i, respectively. Then it is assumed that P, the manipulator, can be divided into two independent linear systems P_1 and P_2. P_i is defined as a combination of the motor i and a constant inertial load. We design K_i and Q_i for these models. Of course, strictly speaking, the equation of a 2 DOF manipulator cannot be decoupled in such a way. However, it is well-known that the decoupling is applicable to position control of a manipulator with continuous-valued PID control under some constraints on the controller gain parameters [30]. For the simplicity of the implementation of the control algorithms in the experimental setups, we adopt this decoupling method. When more precise modeling is required, a quantizer design method for nonlinear P and K is available [23].

We set the gain parameters for PID controllers K_1 and K_2 as listed in Table 5, and the parameters of the quantizers Q_1 and Q_2 as listed in Table 6. Note that, due to the difference between the actual P and the combination of P_1 and P_2, the obtained quantizer is not necessarily optimal in the sense of output error. We do not focus on the strict evaluation of control performance in this section, which was already confirmed in Section 3. Instead, we focus on the dispatching of power packets based on the demand of each motor.

As is mentioned in the introduction, our target systems are disconnected from the external grid. They have limitations on the maximum rate of instantaneous power transferred by a power packet due to the capacity of the source, power lines, and so on. For the control of multiple loads under such a constraint, a demand response can be a solution. In the experimental setup explained above, power packets from one source can be supplied to two loads. Such an overlapping supply occurs with the set of $s_i(k)$ marked with an underscore in Table 4. To represent the limitation of the supply, we set an additional case for experiments, where the overlapping supply is prohibited. This idea is based on the TDM feature of the power packet dispatching system. Because the power supply is represented by a density flow, some time intervals are used to supply and others not. We expect that the unused time intervals are utilized instead of the overlapping supplies.

As a software realization of the limitation, we introduce a supply selector to the controller of the subsystems. The supply selector limits the maximum number of motor supplied by a power packet to just one. This is realized by a communication between the controllers of the two subsystems. When the computation of the controller results in the overlapping $|s_1(k)| = |s_2(k)| = 10$, the selector takes the one which has larger angle error $|\theta_{t,i} - \theta_i|$ at that time instant. The request of the selected motor remains as it is and of the other is renewed by zero.

In the following experiments, we set two cases: (case I) without selector and (case II) with selector. There is no difference in the setup except for the selector. We first confirm the achievement of the manipulator control by power packets through case I, and then present a demand response operation through case II.

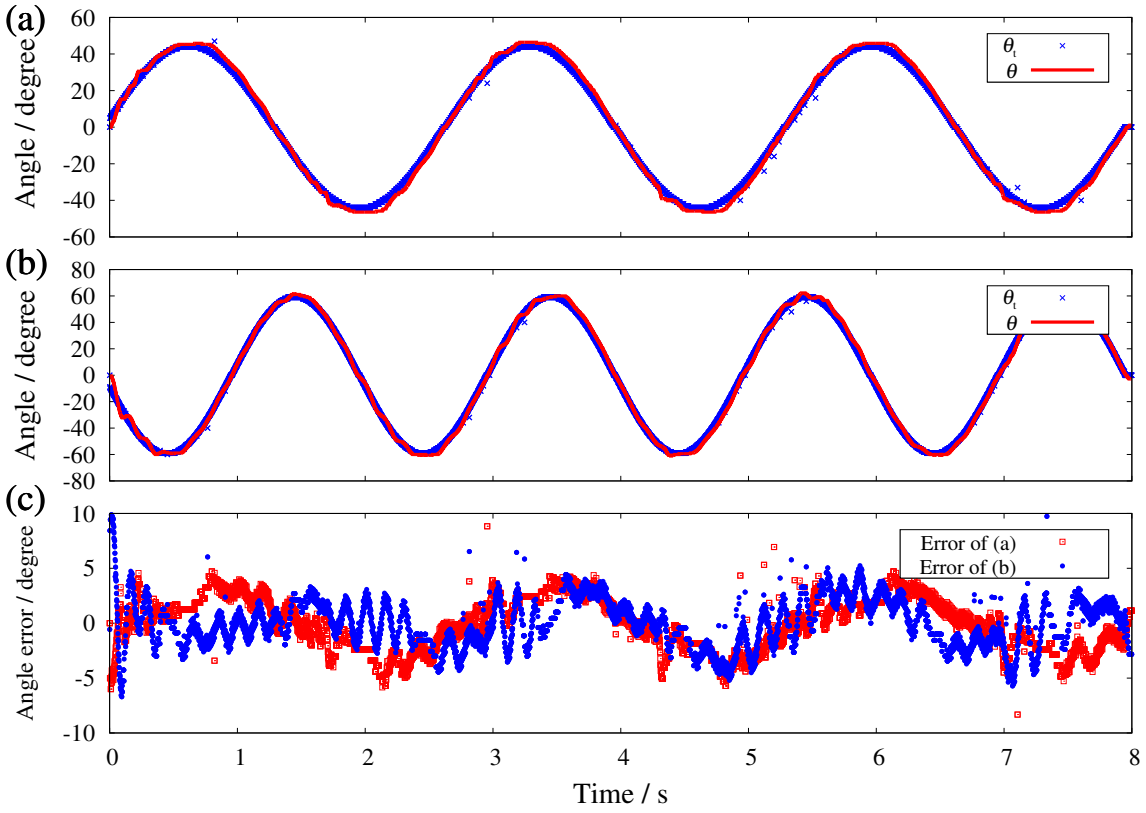

Figure 15: Angle trajectories of case I (without selector). (a) Motor 1: measured angle trajectories and their targets. (b) Motor 2: measured angle trajectories and their targets. (c) Difference between measured trajectories and their targets.

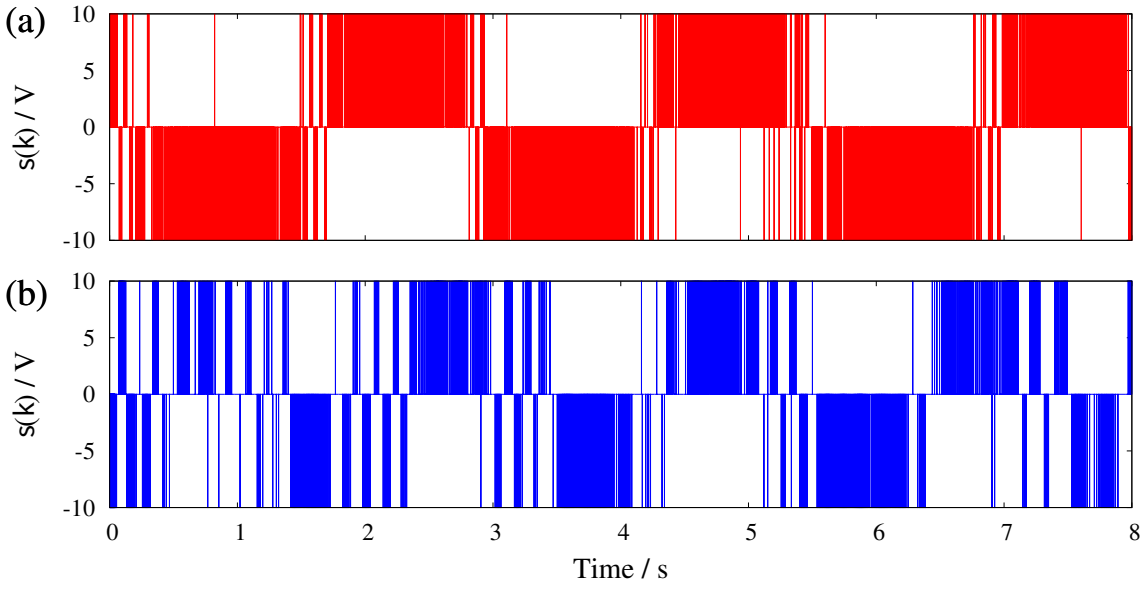

Figure 16: Input sequences in case I (without selector). (a) $s_1(k)$ of motor 1. (b) $s_2(k)$ of motor 2.

Table 7: Number of overlapping, one-side and no power packet supply in experiment of Case I (without selector).

Supply status	Number of supplies
Overlapping : $\lvert s_1(k)\rvert + \lvert s_2(k)\rvert = 20$	211
One-side: $\lvert s_1(k)\rvert + \lvert s_2(k)\rvert = 10$	3593
No supply: $\lvert s_1(k)\rvert + \lvert s_2(k)\rvert = 0$	6197

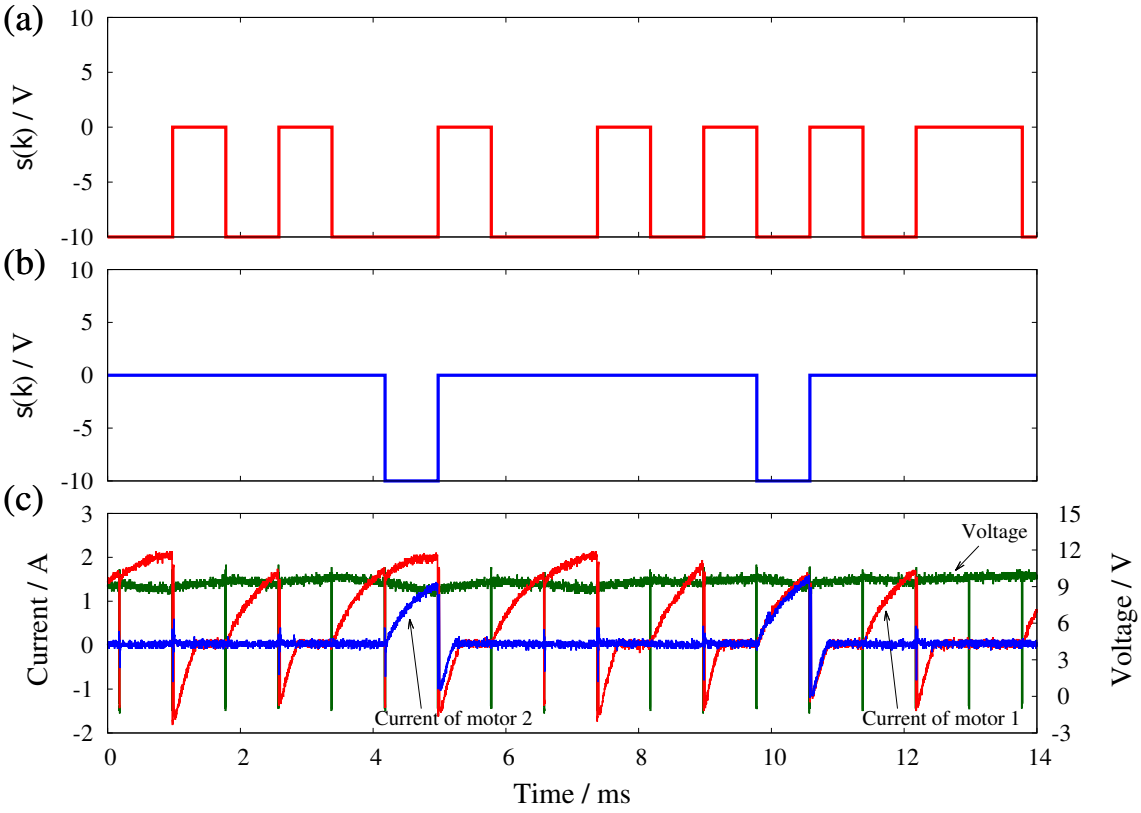

Figure 17: Voltage and current sequence measured in case I (without selector). (a) $s_1(k)$ of motor 1 in enlarged view. (b) $s_2(k)$ of motor 2 in enlarged view. (c) Input voltage of router and current flowing to motor 1 and motor 2.

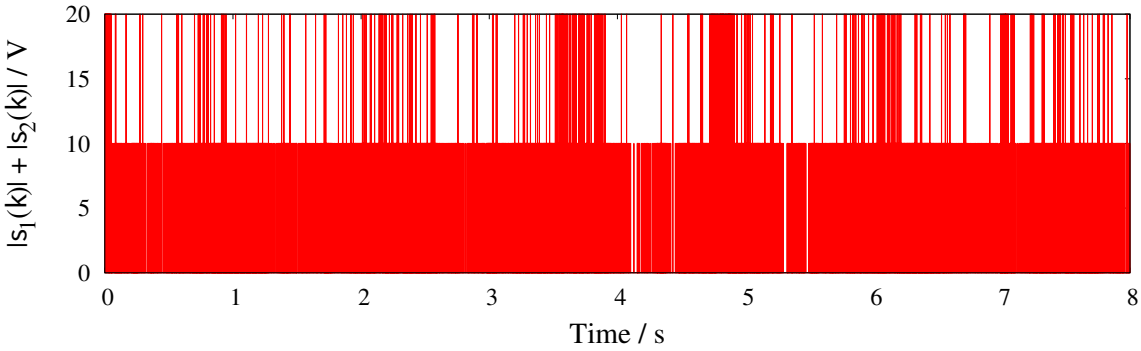

Figure 18: Sum of input sequences in case I (without selector).

4.2 Results and Discussion

4.2.1 Case I

First, let us confirm the successful transfer of signals by power packets. Figure 14 shows a voltage waveform of a header of a power packet. The header indicates the logic sequence "101 0000 000101010." That is, the target angle of the motor 1 at that time instant is 42°. In this way, the target angle of the motors is transferred to the controller of the subsystems. In Figs. 15 (a) and (b), blue plots show the target angle trajectories. Note that the targets in the figures are what the router recognized based on the transferred tags, not what was given to the controller of the packet generator. We can see the sinusoidal targets are transferred correctly in almost all the power packets, although they sometimes deviate from sinusoidal curves of Eq. (12). The deviation is due to a variable computation time of the controller of the packet generator. The software implementation of the target trajectory generation, i.e. the computation of the sinusoidal functions, does not guarantee its real-time operation. Thus, the logic sequence of the tag is sometimes revised just while the packet generator is outputting the bit that is subject to the revision. The errors can be removed by an introduction of a real-time computing technique.

Next, we confirm the achievement of the trajectory control. In Figs. 15 (a) and (b), the joint angles

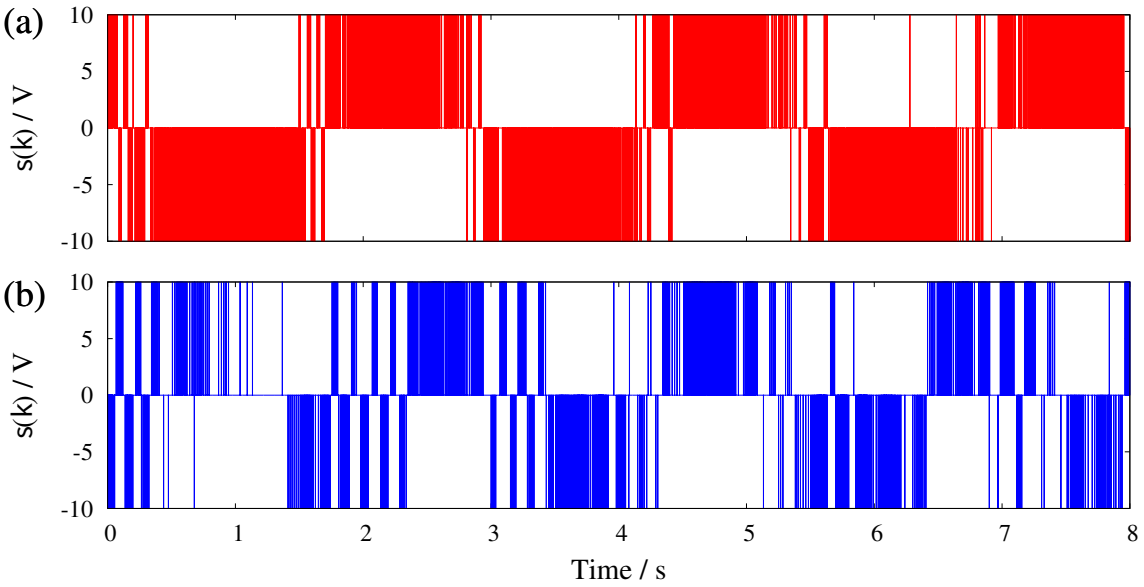

Figure 19: Input sequences in case II (with selector). (a) $s_1(k)$ of motor 1. (b) $s_2(k)$ of motor 2.

follow their targets successfully. In fact, Figs. 15 (c) shows that the absolute error between the target and the measured is at most 5° degrees except for the beginning of the experiment. The average error for the whole experiment time is 2.0° and 1.8° for the motor 1 and the motor 2, respectively. Although we cannot evaluate them with a theoretical reference as mentioned in Section 4.1, the average error is smaller than the mechanical uncertainty caused by a backlash (see Section 3.3). Moreover, the major part of the error appears as a certain delay and an overshoot from the target. They are caused by the limited performance of PID control in trajectory control: the finite response time and the trade-off between fast response and a small overshoot. From these perspectives, we conclude that the trajectory control was achieved with packetized input. We emphasize again that the important point is the comparison of the performance in case I and case II, which is presented in the next subsection.

Now we confirm the transfer of power packets based on the control signals $s_i(k)$. Figure 16 shows the input sequences $s_1(k)$ and $s_2(k)$. Comparing the signal sequences $s_i(k)$ in Fig. 16 and the angle trajectories in Fig. 15, it is confirmed that the sign and the density of the power packet supply are controlled according to the acceleration/deceleration of the motors. Figure 17 shows the enlarged input sequences and the voltage and current waveforms in the corresponding time interval. The voltage is measured across the input terminals of the H bridge modules (common for each), and the current is measured at the plus side of the terminals. We can see that current pulses occur in accordance with the input sequences. From the results, we can confirm that the experimental setup successfully dispatched power packets based on the target signal transferred by information tags and the request of the controller. Note that the position of the current measurement is before the H bridge modules [8], so no matter what the sign of $s_i(k)$ is, there appears no difference in the current waveforms. The direction of the motor current can be identified by comparing them with the input sequences, $s_i(k)$.

Now Fig. 17 indicates that the overlapping supply to motor 1 and motor 2 sometimes occurred. Figure 18 shows the sum of absolute inputs $|s_1(k)| + |s_2(k)|$ for the entire experiment. The values 20, 10 and 0 in the figure indicate that the overlapping, one-side and no power supplies occurred at the time intervals, respectively. Table 7 shows the number of these supplies for the whole experimental time. The overlapping transfer occurred in more than 200 time slots, while there were more than 6000 empty time slots. This result is not ideal from the perspective of the instantaneous power concentration, which might result in an exceed of the limitation of the power source. Through the following experiment of case II, we confirm that the selector can be a solution for this problem.

4.2.2 Case II

Figure 19 shows the input sequences of case II. The qualitative tendency of the change of the density according to the acceleration/deceleration is same as in the case I. However, the sequence differs in detail. Figure 20 shows the sum of absolute inputs $|s_1(k)| + |s_2(k)|$. We can confirm that there is no simultaneous supply in any time slots. Table 8 shows the number of each supply status during the experiment. Compared

[8] This is different from the measurement position of the experiment in Section 3.

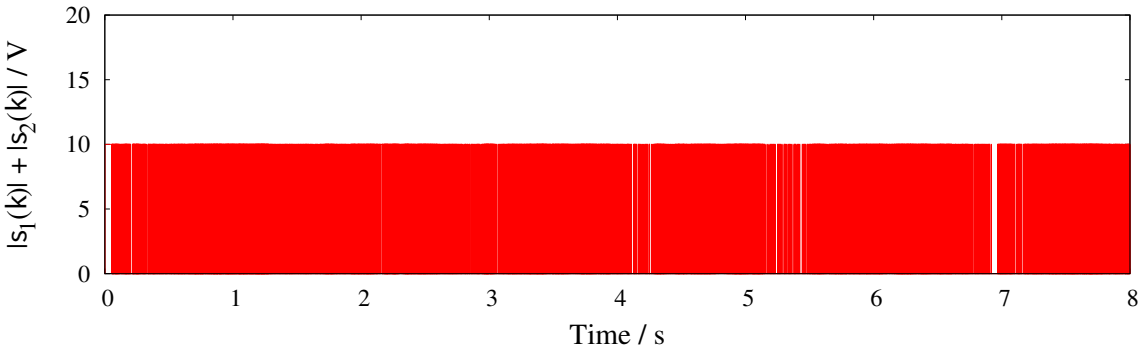

Figure 20: Sum of input sequences in case II (with selector).

Table 8: Number of overlapping, one-side and no power packet supply in experiment of case II (with selector).

Supply status	Number of supplies
Overlapping : $\|s_1(k)\| + \|s_2(k)\| = 20$	0
One-side: $\|s_1(k)\| + \|s_2(k)\| = 10$	3874
No supply: $\|s_1(k)\| + \|s_2(k)\| = 0$	6127

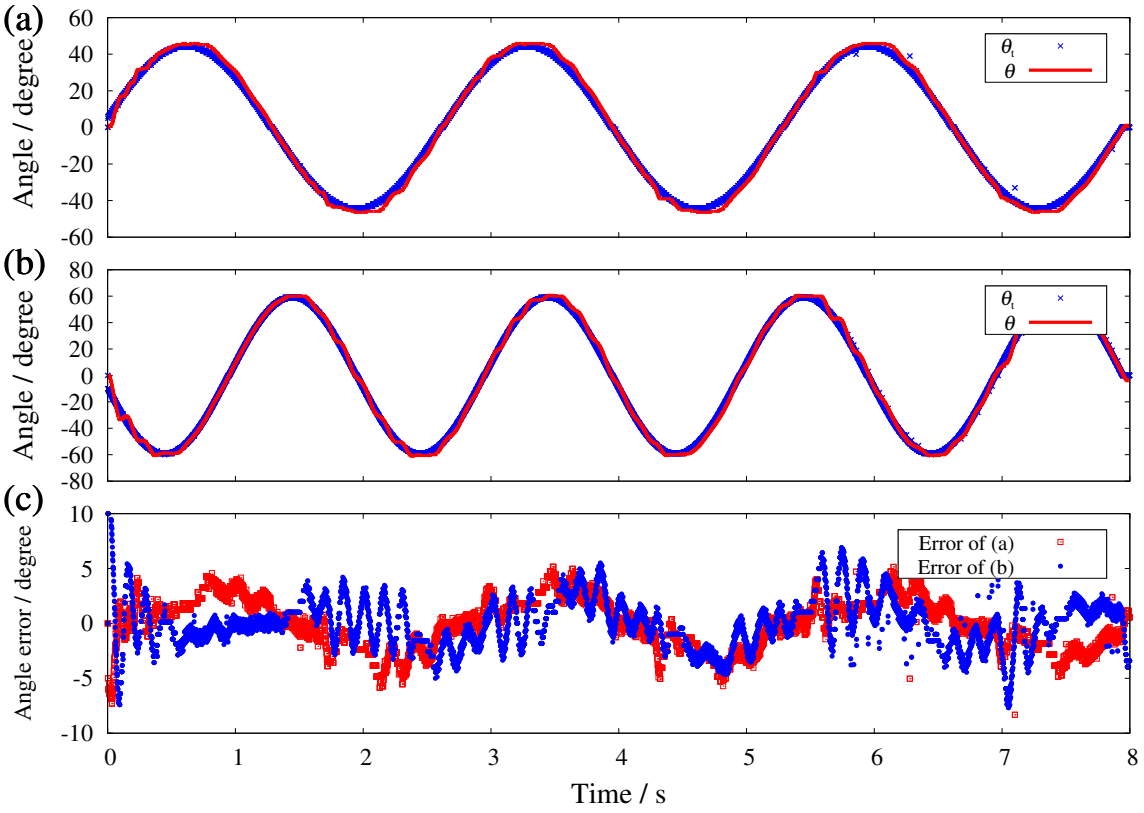

Figure 21: Angle trajectories of case II (with selector). (a) Motor 1: measured angle trajectories and their targets. (b) Motor 2: measured angle trajectories and their targets. (c) Difference between measured trajectories and their targets.

with the results in case I, the number of one-side supplies is increased by 281. They compensate the simultaneous supplies of 211 times in case I.

In spite of the modification of the power packet sequences, there appears no remarkable degradation of the control performance. Figure 21 shows the angle trajectories measured in case II. Although some error occurred for the same reasons with those in case I, the angle trajectories follow the target successfully. In fact, the average absolute error of the motor 1 and the motor 2 are 1.9° and 1.8°, respectively. From the perspective of the angle error, we conclude that no performance degradation occurred with the selector implemented. The modification of power packet sequence by the demand response operation with the selector successfully reduced the amount of instantaneous power without affecting the control performance.

5 Conclusions

In this paper, we proposed the decentralized subsystem for packet-based feedback control. With the application of the proposed scheme to angle control of a dc motor, the successful operation was confirmed numerically and experimentally. Then, we presented the application to the manipulator drive. The experiments showed the achievement of successful trajectory control and the peak-power reduction based on the demand response operation of the subsystems.

The proposed scheme can be applied to a dispatching system for a robot manipulator with more DOFs by simple expansion. In the simplest way, the proposed subsystems are connected in parallel to form a router for motor drive. The parallel addition of a subsystem is available as long as there are unused time slots for power packets available (see Tables 7 and 8). For systems with more DOFs, it is also possible to install multiple sources and a network of routers between the sources and the loads. An appropriate construction of the network can provide multiple paths for a power packet transfer [9], which contributes to an increased transfer capacity of the dispatching network. Now note that the proposed system is applicable even when a robot manipulator is equipped with motors of different power and voltage ratings for each DOF. The TDM transfer enables to handle power packets of different voltage and/or power ratings in the same dispatching network without putting additional power converters [11].

As is mentioned above, the notion of a transfer capacity of a power dispatching network is important in the design of a power packet dispatching network. It tells us the maximum number of loads that can be driven by a given dispatching network. Conversely, when the type and the number of loads are given, it suggests how many paths the network needs to have, for example. However, we have so far used an ad hoc methodology to determine the structure of a dispatching network. A general formulation for a capacity estimation is thus one of the future research direction. A challenge is that there are many factors to be considered. They include voltage levels of the sources, a unit time length of a power packet, and a maximum time interval during which a load can stand without a supply [9]. It might be a good way to begin with a simplified problem by fixing some of them, and then to expand it to more general problems.

In this paper, we assumed the two motors have the same ratings and thus the voltage amplitude of all power packets is identical. However, in a general dispatching system with multiple power sources, the sources can have different voltage levels. In addition, from the viewpoint of control, the existence of different voltage levels in a network also has a potential to provide another advantage. For example, let us consider the case where a wrist joint of a manipulator is required to move quickly, and the power source for a base joint of the manipulator, which has a larger voltage level than for the wrist, can afford to supply another load as well. The initial response speed of the wrist can be enhanced by the use of power packets of the larger voltage level at the beginning of a whole movement. On the contrary, at the final stage of the movement, the wrist movement become slow and thus a precision is more important than the quick response. In this stage, power packets of the lower voltage are more suitable. From these perspectives, a modification of the proposed control scheme to include such a selection of power sources can be an interesting future direction. Now note that, in the power packet dispatching system, it is not a good way to prepare redundant sources for each of loads. It is not acceptable in some of our target applications such as vehicles because it increases the weight and volume of the system significantly. Instead, we consider the case where the loads can share the sources that usually supply their own loads. The point is that the redundancy is not provided for each of the loads, but for the whole system.

The proposed scheme can also be applied to a dispatching network for distributed robots and/or any other (groups of) loads. Let us now consider a network depicted in Figure 22 as an example. The network consists of sub-networks, which have a similar configuration with the dispatching system discussed in Section 4. One point that should be noted is that the packet generator is replaced by a router that connects a sub-network to others as well as its local sources [10]. Thus, a part of power can be from other sub-networks. This configuration is for a power sharing among sub-networks, which increases the performance of the whole system compared to the case where the sub-networks are disconnected from each other. As is presented in the experimental results of Section 4, some time slots are not used for a power supply. They can be shared with other sub-networks that have an instantaneous shortage of power due to, for example, a heavy duty on multiple joints of the manipulator. To introduce such a network, a part of the proposed scheme regarding the packet generation should be modified. In the scheme at the routers, a source selection algorithm is required. The algorithm assigns the power requested from loads to the sources; which is called an upstream dispatching of power packets [31, 32]. The proposed scheme regarding the RMDs is implemented similarly with the setup in this paper.

[9] The time interval is related largely to the specification of the load such as electrical and mechanical time constants in the case of a robot manipulator. If the interval is sufficiently shorter than the time constants, the fluctuation of states such as the angle is expected to be small.

[10] A router configuration for multiple input/output has been presented in [9]. In the study, the power packet routing via multi-stage routers in a dispatching network has also been confirmed in experiments.

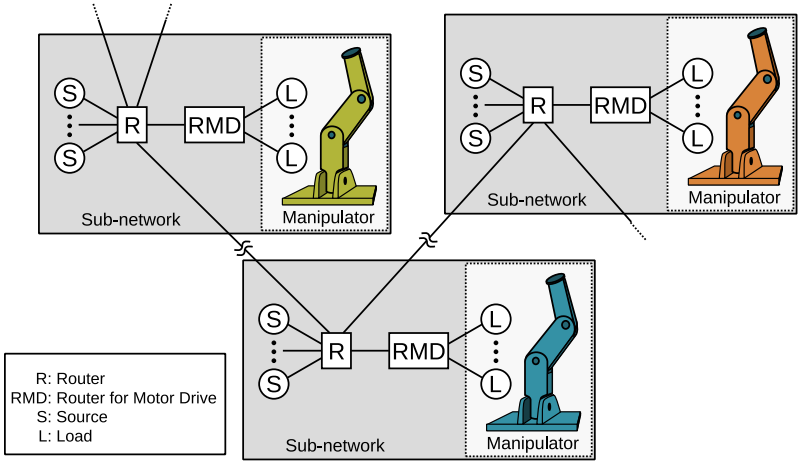

Figure 22: Dispatching network for distributed robots.

The motors used in the experiments are for a hobby use and their power ratings are relatively small. However, the proposed scheme is applicable to general loads that can be modeled by a state-space representation. In addition, the hardware setup of the power packet dispatching system has a potential to handle power transfer of much larger ratings. We have already confirmed that synchronous motors of kW-order ratings for an industrial use can be controlled by power packets supplied in an open-loop manner [11]. The next step will be the modification of the control scheme for such multi-phase motors. We consider that our previous studies on stepper motor drives by power packets [14] [15] will give a clue for the solution.

Here, note that the software of the developed subsystem is still subject to future improvement. For example, the results of Section 3 show that the unnecessary oscillation of $s(k)$ occurred especially while the angle was near the target. Such an oscillation is not ideal from the perspective of the energy efficiency. A solution to improve the efficiency would be a replacement of the evaluation function (6) with quadratic function of both state and input variable [33].

The target of this research is the decentralized control of the flow of power packets based on the convenience of both the sources and the loads. The demand response operation in Section 4 is an example to present the possibility. Here, we put an emphasis on the importance of the physical integration of the transfer of power and information. The discrepancy of an actual power flow (physical quantity) and its virtual flow computed in cyber world (information) results in a critical failure of the whole power system. From this viewpoint, the power packet dispatching system is a promising candidate for the realization of the decentralized processing of power and information, especially in applications with a limited power capacity.

A Numerical models of P and K

The coefficient matrices for state space expression of P are

$$P_{\mathrm{a}} = \begin{bmatrix} 2.9404 \times 10^{-1} & 0 & -4.3308 \times 10^{-2} \\ 6.1610 \times 10^{-5} & 1.0000 & 7.9501 \times 10^{-4} \\ 1.2823 \times 10^{-1} & 0 & 9.8598 \times 10^{-1} \end{bmatrix}, \quad P_{\mathrm{b}} = \begin{bmatrix} 2.1026 \times 10^{-1} \\ 8.1673 \times 10^{-6} \\ 2.8005 \times 10^{-2} \end{bmatrix}, \tag{13}$$

$$P_{\mathrm{c1}} = \begin{bmatrix} 0 & 1 & 0 \\ 0 & 0 & 1 \end{bmatrix}, \quad P_{\mathrm{c2}} = \begin{bmatrix} 0 & 1 & 0 \end{bmatrix}. \tag{14}$$

The coefficient matrices for state space expression of K are

$$K_{\mathrm{a}} = 1.0000, \quad K_{\mathrm{b1}} = T, \quad K_{\mathrm{b2}} = \begin{bmatrix} -T & 0 \end{bmatrix}, \quad K_{\mathrm{c}} = K_{\mathrm{i}}, \tag{15}$$

$$K_{\mathrm{d1}} = K_{\mathrm{p}}, \quad K_{\mathrm{d2}} = \begin{bmatrix} -K_{\mathrm{p}} & -K_{\mathrm{d}} \end{bmatrix}. \tag{16}$$

Acknowledgments

This work was partially supported by JSPS KAKENHI Grant Number JP18J11530, by Cross-ministerial Strategic Innovation Promotion Program from New Energy and Industrial Technology Development Or-

ganization, and by the Super Cluster Program from Japan Science and Technology Agency. The authors would like to thank Dr. Ryo Takahashi for his fruitful discussions.

References

[1] Seok S, Wang A, Chuah MYM, et al. Design Principles for Energy-Efficient Legged Locomotion and Implementation on the MIT Cheetah Robot. *IEEE/ASME Trans Mechatron* 2015; 20(3): 1117–1129.

[2] Kumar L, Jain S. Electric propulsion system for electric vehicular technology: A review. *Renew Sustain Energy Rev* 2014; 29: 924–940.

[3] Tie SF, Tan CW. A review of energy sources and energy management system in electric vehicles. *Renew Sustain Energy Rev* 2013; 20: 82–102.

[4] Sarlioglu B, Morris CT. More Electric Aircraft: Review, Challenges, and Opportunities for Commercial Transport Aircraft. *IEEE Trans Transport Electrific* 2015; 1(1): 54–64.

[5] Toyoda J, Saitoh H. Proposal of an Open-electric-energy-network (OEEN) to Realize Cooperative Operations of IOU and IPP. In: *Proc Int Conf Energy Management Power Delivery*; 1998; Singapore: 218–222.

[6] Nakayama K, Zhao C, Bic LF, Dillencourt MB, Brouwer J. Distributed power flow loss minimization control for future grid. *Int J Circ Theor Appl* 2015; 43(9): 1209–1225. doi: 10.1002/cta.1999

[7] Kurokawa F, Wang J. Topics of digital control approaches for future-oriented power converters. *Nonlinear Theor Its Appl, IEICE* 2018; 9(3): 306–321. doi: 10.1587/nolta.9.306

[8] Takuno T, Koyama M, Hikihara T. In-home Power Distribution Systems by Circuit Switching and Power Packet Dispatching. In: *Proc 1st IEEE Int Conf Smart Grid Commun*; 2010; Gaithersburg, MD, USA: 427–430.

[9] Takahashi R, Tashiro K, Hikihara T. Router for Power Packet Distribution Network: Design and Experimental Verification. *IEEE Trans Smart Grid* 2015; 6(2): 618–626.

[10] Takahashi R, Azuma S, Hasegawa M, Ando H, Hikihara T. Power Processing for Advanced Power Distribution and Control. *IEICE Trans Commun* 2017; E100.B(6): 941–947. doi: 10.1587/transcom.2016EBN0005

[11] Mochiyama S, Okuda T, Hikihara T. Power packet dispatching with shared power line for connection of multiple sources and loads. Submitted.

[12] Fadali M, Visioli A. *Digital control engineering: analysis and design*. MA, USA: Academic Press. 2013.

[13] Takahashi R, Azuma S, Hikihara T. Power Regulation with Predictive Dynamic Quantizer in Power Packet Dispatching System. *IEEE Trans Ind Electron* 2016; 63(12): 7653–7661.

[14] Mochiyama S, Takahashi R, Hikihara T. Trajectory control of manipulator fed by power packets. *Int J Circ Theor Appl* 2017; 45(6): 832–842.

[15] Mochiyama S, Takahashi R, Hikihara T. Close-loop Angle Control of Stepper Motor Fed by Power Packets. *IEICE Trans Fundam Electron, Commun Computer Sciences* 2017; E100-A(7): 1571–1574.

[16] Mochiyama S, Hikihara T. Experimental Implementation of Power Packet Density Modulation to Close-loop Control of Manipulator. In: Proc Int Symp Power Electron, Electr Drives, Autom, Motion; 2018; Amalfi, Italy: 763–768.

[17] Orcioni S, d'Aparo R, Lobascio A, Conti M. Dynamic OSR dithered sigma-delta modulation in solid state light dimming. *Int J Circ Theor Appl* 2013; 41(4): 387–395.

[18] Sadanda Y, Okuda T, Hikihara T. Direct drive of a buck converter by delta-sigma modulation at 13.56-MHz sampling. In: *Proc IEEE Workshop Contr Model Power Electron*; 2017: 1–4

[19] Kimoto T. Material science and device physics in SiC technology for high-voltage power devices. *Japan J Appl Phys* 2015; 54(4): 040103.

[20] Sugano R, Sun Y, Sekiya H. High-frequency resonant gate driver with isolated class-E amplifier. *Nonlinear Theor Its Appl, IEICE* 2018; 9(3): 358–373. doi: 10.1587/nolta.9.358

[21] Azuma S, Minami Y, Sugie T. Optimal Dynamic Quantizers for Feedback Control With Discrete-Level Actuators: Unified Solution and Experimental Evaluation. *J Dynam Syst, Meas, Contr* 2011; 133(2).

[22] Morita R, Azuma S, Minami Y, Sugie T. Graphical Design Software for Dynamic Quantizers in Control Systems. *SICE J Contr, Meas, Syst Integr* 2011; 4(5): 372–379. doi: 10.9746/jcmsi.4.372

[23] Azuma S, Sugie T. Dynamic Quantization of Nonlinear Control Systems. *IEEE Trans Autom Contr* 2012; 57(4): 875-888. doi: 10.1109/TAC.2011.2167824

[24] Azuma S, Sugie T. Synthesis of Optimal Dynamic Quantizers for Discrete-Valued Input Control. *IEEE Trans Autom Contr* 2008; 53(9): 2064–2075.

[25] Minami Y, Azuma S, Sugie T. An optimal dynamic quantizer for feedback control with discrete-valued signal constraints. In: *Proc 46th IEEE Conf Dec Contr*; 2007: 2259–2264

[26] Digilent Inc. DC Motor/Gearbox (1:53 Gear Ratio): Custom 6V Motor Designed for Digilent Robot Kits. 2014.

[27] Digilent Inc. Pmod HB5: H-bridge Driver with Feedback Inputs. 2016.

[28] SeDuMi: A linear/quadratic/semidefinite solver for Matlab and Octave.

[29] Zhou Y, Takahashi R, Fujii N, Hikihara T. Power packet dispatching with second-order clock synchronization. *Int J Circ Theor Appl* 2015; 44(3): 729–743.

[30] Arimoto S. *Control Theory of Non-linear Mechanical Systems : a Passivity-based and Circuit-theoretic Approach*. Oxford University Press. 1996.

[31] Bialek J. Tracing the flow of electricity. *IEE Proceedings — Generation, Transmission and Distribution* 1996; 143 (4): 313–320.

[32] Nawata S, Takahashi R, Hikihara T. Up-stream dispatching of power by density of power packet. *IEICE Trans Fundam Electron Commun Comput Sci* 2016; E99-A (12): 2581–2584.

[33] Anderson BDO, Moore JB. *Optimal control: linear quadratic methods*. Englewood Cliffs, NJ: Prentice-Hall, Inc. 2007.